Numerical Heat Transfer, Part A, 36:115–128, 1999

1040–7782/99 $12.00+ .00

PASSIVE HEAT TRANSFER AUGMENTATION IN A CYLINDRICAL ANNULUS UTILIZING A POROUS PERTURBATION

S. V. Iyer and K. Vafai
Department of Mechanical Engineering, Ohio State University, Columbus, Ohio 43210, USA

In this work, free convective fluid flow and heat transfer are analyzed in a horizontal cylindrical annulus in the presence of a porous geometric perturbation. The flow in the porous region is modeled using the Brinkman-Forchheimer-Darcy model. The numerical scheme used in the present study is based on a Galerkin method of the finite element formulation. The nature of the three-dimensional flow field has been analyzed in detail, and the local and average Nusselt numbers have been obtained for a range of Rayleigh numbers of practical interest. In order to evaluate the effect of a porous perturbation, the flow and heat transfer characteristics were compared with those for a regular annulus without a perturbation and one with a solid perturbation. This study reports on the dependence of the flow and heat transfer characteristics on the governing parameters such as the ratio of the conductivity of the porous material to that of the fluid and the permeability. A correlation has been obtained that captures the variations of the overall heat transfer as a function of the Rayleigh number, the permeability, and the conductivity ratio. The results of this study show that both heat transfer retardation and enhancement can be achieved with the introduction of a porous perturbation.

INTRODUCTION

From a practical point of view, there is an interest in determining the buoyancy-induced fluid flow and heat transfer fields in an annulus in the presence of a porous substrate. This interest is due to the possibility of heat transfer augmentation in various applications, such as underground cable systems, thermal energy storage systems, aircraft brake systems, and geothermal-operation activities.

There have been some analytical studies dealing with the natural convection induced flow and heat transfer in a horizontal concentric annulus filled with a porous medium. Rao et al. [1] performed a steady and transient analytical investigation in a horizontal porous annulus heated from the inner surface. The studies were carried out for a radius ratio of 2.0 with Ra Da numbers ranging from 1 to 300. Based on the initial condition, three families of convergent solutions were found to appear one after another with increasing Ra Da numbers. They found the existence of a critical Ra Da number at which two modes were having quite different flow structures, but the same overall heat transfer rate. In the higher Ra Da region, overall heat transfer rates calculated from multicellular flows were found to agree well with experimental data. Pop et al. [2] used the method of

Received 21 October 1998; accepted 11 January 1999.
Address correspondence to Dr. Kambiz Vafai, Department of Mechanical Engineering, Ohio State University, 206 W. 18th Avenue, Columbus, OH 43210-1107, USA.

NOMENCLATURE

c_p	specific heat, kJ kg^{-1} K^{-1}	x^*	dimensionless length of the perturbation in the axial direction
D_1	diameter of inner cylinder, m	α	thermal diffusivity, m^2 s^{-1}
D_2	diameter of outer cylinder, m	β	volume expansion coefficient, K^{-1}
D_p	diameter of the perturbation, m	κ	permeability of the porous medium, m^2
Da	Darcy number ($= \kappa/D_2^2$)	μ	dynamic viscosity, m^2 s^{-1}
g	acceleration due to gravity, m s^{-2}	$\tilde{\mu}$	effective viscosity, m^2 s^{-1}
k	thermal conductivity, W m^{-1} K^{-1}	ν	kinematic viscosity, kg m^{-1} s^{-1}
L	axial length of entire annulus, m	ρ	density, kg m^{-3}
n	outward drawn normal	ϕ	porosity of the porous medium
Nu	Nusselt number		
p	pressure, Pa		
Pr	Prandtl number ($= \nu/\alpha$)	**Subscripts**	
r^*	dimensionless length in the radial direction ($= h_p/G$)	e	effective value
R_1	radius of the inner cylinder, m	f	fluid
R_2	radius of the outer cylinder, m	p	perturbation
Ra	Rayleigh number	r	r component
	$[= g\beta\Delta T(R_2 - R_1)^3/\alpha\nu]$	s	solid
T	temperature, K	x	x component
u_r	velocity in the r direction, m s^{-1}	θ	θ component
u_x	velocity in the x direction, m s^{-1}	1	inner cylinder
u_θ	velocity in the θ direction, m s^{-1}	2	outer cylinder
x, r, θ	cylindrical coordinates	∞	condition at infinity

matched asymptotic expansions to study the problem of transient natural convection in a horizontal concentric porous annulus with the inner and outer cylinders being maintained at uniform temperatures. The analytical solution showed that the short time solution was significantly different from the steady state solution. The flow was found to consist of three distinct regions: an inner boundary layer adjacent to the inner surface, an outer boundary layer adjacent to the outer surface, and a core region between the two boundary layers.

Charrier-Mojtabi et al. [3] carried out an experimental and numerical study of multicellular free convection flows in an annulus filled with a porous medium. They solved the two-dimensional (2-D) Darcy-Boussinesq model using two different numerical methods, namely, the Fourier-Galerkin and the collocation-Chebyshev methods. The collocation-Chebyshev method was found to give a better accuracy, especially for the description of the boundary layers developed near the inner and outer cylinders. The computations were carried out for a range of Ra and radius ratios. For unicellular flows the results obtained by the two methods were found to be in good agreement. For bicellular, tricellular, and multicellular flows the collocation-Chebyshev method was found to present better spatial radial accuracy. The experimental study showed the existence of bicellular 2-D structures, and in general, good agreement was seen with the numerical results. Vasseur et al. [4] numerically studied the problem of natural convection in an annular porous layer with internal heat generation. At low Ra, a parabolic temperature profile was

seen across the annulus, resulting in two counterrotating vortices in each half cavity. In the pseudoconduction regime the effect of the internal heat source was to heat up the core fluid. The maximum temperature within the porous medium was found to be considerably higher than that induced by pure conduction. A flow structure consisting of a thermally stratified core and two boundary layers was obtained at high Ra from both analytical and numerical analyses.

Studies dealing with non-Darcian effects have also been carried out. Muralidhar and Kulacki [5] carried out a computational study of free convective flow and heat transfer in a horizontal annulus filled with a porous medium. The outer wall was held at a constant temperature, while both isothermal and constant heat flux boundary conditions were considered on the inner walls. The non-Darcian effects, such as inertial and viscous forces, as well as the variation of porosity, were included in the calculations. Average Nusselt numbers were obtained for the Ra Da range from 20 to 4000 for the case of isothermal boundaries, and 20 to 20,000 for the case of the inner wall heated by a constant heat flux. Over the range of parameters considered, the inertial and viscous friction in the fluid phase was found to have a negligible effect on the Darcy flow, while the variable porosity was seen to produce channeling near the wall. Vafai and Kim [6] numerically studied the convective flow and heat transfer through a composite porous/fluid system. The composite medium consisted of a fluid layer overlaying a porous substrate, which is attached to the surface of a plate. The effects of governing parameters, such as the Da, inertial parameter, Pr, and conductivity ratio of the porous material to that of the fluid, were investigated. The porous substrate was found to significantly reduce the frictional drag and heat transfer rate at the wall. Vafai and Kim showed that both heat transfer retardation and enhancement could be achieved through the attachment of a porous substrate. This same effect is also seen to be the case for the present work. Ettefagh et al. [7] analyzed the importance and relevance of non-Darcian effects associated with buoyancy-driven convection in open-ended cavities filled with a fluid-saturated porous medium. The significance of inertia and boundary effects, and their influence on the prediction of buoyancy-induced flow and heat transfer, were investigated.

To the best of the authors' knowledge, there have been no studies concerning the effect of porous geometric modifications on the concentric cylindrical annuli. Iyer and Vafai [8, 9] have addressed the issue of the single and multiple solid perturbations on the 3-D buoyancy-driven flow and heat transfer in an annular cavity. The general patterns and detailed features of the flow and heat transfer in the annulus were presented, and considerable deviation from the coaxial double-helical flow pattern was observed.

In the present work a qualitative and quantitative understanding of the flow field and heat transfer process in an annulus subjected to a porous perturbation on the inner cylinder is provided. The effects of variations in matrix to fluid thermal conductivities and variations in Da are studied. Also, a comparison between porous and solid perturbations is performed. The heat transfer behavior is studied by looking at the variations in the average and local Nu on the inner and outer cylinders. The full 3-D Navier-Stokes equation is numerically solved using the Galerkin weighted residual method of the finite element formulation.

FORMULATION

Physical Model and Assumptions

The physical model and coordinate system used in the present study is shown in Figure 1. The perturbation is placed symmetrically on the inner cylinder of the annulus. The flow is expected to be symmetric with respect to the vertical circumferential plane, a point verified by computational simulations.

In the numerical analysis, the thermophysical properties of the walls and the fluid are assumed to be independent of temperature except for the density in the momentum equation, where the Boussinesq approximation is invoked. The fluid is assumed to be Newtonian and incompressible, and the viscous dissipation in the fluid is neglected. The main objective of this work is to establish the effect of a porous perturbation, and as such, the main flow field and heat transfer characteristics of interest for a range of applications can be captured for results presented up to a Ra of 10^4.

Governing Equations

The problem is modeled as a 3-D, steady state, natural convection for an incompressible fluid. The nondimensional governing equations [7] for the porous region are as follows.

Continuity

$$\frac{\partial u_r}{\partial r} + \frac{u_r}{r} + \frac{1}{r}\frac{\partial u_\theta}{\partial \theta} + \frac{\partial u_x}{\partial x} = 0 \tag{1}$$

x momentum

$$\frac{\mu}{\kappa_x} u_x = -\frac{\partial p}{\partial x} + \tilde{\mu}\nabla^2 u_x \tag{2}$$

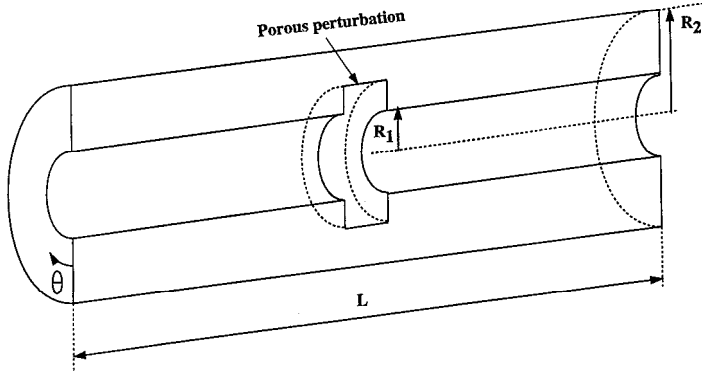

Figure 1. Physical model and coordinate system.

r momentum

$$\frac{\mu}{\kappa_r}u_r = -\frac{\partial p}{\partial r} + \tilde{\mu}\nabla^2 u_r + \left(\frac{\mathrm{Ra}}{\mathrm{Pr}}\right)^{1/2} T\cos\theta \tag{3}$$

θ momentum

$$\frac{\mu}{\kappa_\theta}u_\theta = -\frac{1}{r}\frac{\partial p}{\partial \theta} + \tilde{\mu}\nabla^2 u_\theta + \left(\frac{\mathrm{Ra}}{\mathrm{Pr}}\right)^{1/2} T\sin\theta \tag{4}$$

Energy

$$(\rho c_p)_e\left(u_r\frac{\partial T}{\partial r} + \frac{u_\theta}{r}\frac{\partial T}{\partial \theta} + u_x\frac{\partial T}{\partial x}\right) = k_e\left\{\frac{\partial^2 T}{\partial r^2} + \frac{1}{r}\frac{\partial T}{\partial r} + \frac{1}{r^2}\frac{\partial^2 T}{\partial \theta^2}\right\} \tag{5}$$

In Eqs. (2)–(5), μ is the viscosity of the fluid phase of the porous medium and $\tilde{\mu}$ is an effective viscosity. It has been found that the approximation of setting the effective viscosity of the fluid-saturated porous medium equal to the viscosity of the fluid provides good agreement with experimental data [6]. This approach is adopted in this work. The permeabilities in the x, r, and θ directions are designated as κ_x, κ_r, and κ_θ, respectively. To concentrate on the fundamental aspects, in this work, these permeabilities are taken to be the same. In Eq. (5) the subscript e indicates an effective property whose value needs to be prescribed. The effective thermal properties are related to fluid and solid matrix properties by the following relations:

$$\begin{aligned}(\rho c_p)_e &= \phi\rho c_p + (1-\phi)(\rho c_p)_s \\ k_e &= \phi k + (1-\phi)k_s\end{aligned} \tag{6}$$

where the subscript s refers to solid matrix properties, while those without subscripts are those of the fluid.

The nondimensional governing equations for the fluid are given as follows.

Continuity

$$\frac{\partial u_r}{\partial r} + \frac{u_r}{r} + \frac{1}{r}\frac{\partial u_\theta}{\partial \theta} + \frac{\partial u_x}{\partial x} = 0 \tag{7}$$

x momentum

$$\left(\frac{\mathrm{Ra}}{\mathrm{Pr}}\right)^{1/2}\left(u_r\frac{\partial u_x}{\partial x} + \frac{u_\theta}{r}\frac{\partial u_x}{\partial \theta} + u_x\frac{\partial u_x}{\partial x}\right) = -\frac{\partial p}{\partial x} + \left\{\frac{1}{r}\frac{\partial}{\partial r}\left(r\frac{\partial u_x}{\partial r}\right) + \frac{1}{r^2}\frac{\partial^2 u_x}{\partial \theta^2} + \frac{\partial^2 u_x}{\partial x^2}\right\} \tag{8}$$

r momentum

$$\left(\frac{\mathrm{Ra}}{\mathrm{Pr}}\right)^{1/2}\left(u_r\frac{\partial u_r}{\partial r}+\frac{u_\theta}{r}\frac{\partial u_r}{\partial \theta}-\frac{u_\theta^2}{r}+u_x\frac{\partial u_r}{\partial x}\right)$$

$$=-\frac{\partial p}{\partial r}+\left(\frac{\mathrm{Ra}}{\mathrm{Pr}}\right)^{1/2}(T)\cos\theta$$

$$+\left\{\frac{\partial}{\partial r}\left(\frac{1}{r}\frac{\partial[ru_r]}{\partial r}\right)+\frac{1}{r^2}\frac{\partial^2 u_r}{\partial \theta^2}-\frac{2}{r^2}\frac{\partial u_\theta}{\partial \theta}+\frac{\partial^2 u_r}{\partial x^2}\right\} \tag{9}$$

θ momentum

$$\left(\frac{\mathrm{Ra}}{\mathrm{Pr}}\right)^{1/2}\left(u_r\frac{\partial u_\theta}{\partial r}+\frac{u_\theta}{r}\frac{\partial u_\theta}{\partial \theta}+\frac{u_r u_\theta}{r}+u_x\frac{\partial u_\theta}{\partial x}\right)$$

$$=-\frac{1}{r}\frac{\partial p}{\partial \theta}+\left(\frac{\mathrm{Ra}}{\mathrm{Pr}}\right)^{1/2}(T)\sin\theta$$

$$+\left\{\frac{\partial}{\partial r}\left(\frac{1}{r}\frac{\partial[ru_\theta]}{\partial r}\right)+\frac{1}{r^2}\frac{\partial^2 u_\theta}{\partial \theta^2}+\frac{2}{r^2}\frac{\partial u_r}{\partial \theta}+\frac{\partial^2 u_\theta}{\partial x^2}\right\} \tag{10}$$

Energy

$$\left(\frac{\mathrm{Ra}}{\mathrm{Pr}}\right)^{1/2}\left(u_r\frac{\partial T}{\partial r}+\frac{u_\theta}{r}\frac{\partial T}{\partial \theta}+u_x\frac{\partial T}{\partial x}\right)=\frac{\partial^2 T}{\partial r^2}+\frac{1}{r}\frac{\partial T}{\partial r}+\frac{1}{r^2}\frac{\partial^2 T}{\partial \theta^2} \tag{11}$$

The following dimensionless parameters have been used in the above set of equations, and the superscripts have been dropped for convenience.

$$x^*=\frac{x}{R_2}\qquad r^*=\frac{r}{R_2} \tag{12}$$

$$u_x^*=\frac{u_x R_2}{\alpha(\mathrm{Ra}\ \mathrm{Pr})^{1/2}}\qquad u_r^*=\frac{u_r R_2}{\alpha(\mathrm{Ra}\ \mathrm{Pr})^{1/2}}\qquad u_\theta^*=\frac{u_\theta R_2}{\alpha(\mathrm{Ra}\ \mathrm{Pr})^{1/2}} \tag{13}$$

$$T^*=\frac{T-T_\infty}{T_1-T_\infty}\qquad p^*=\frac{pR_2^2}{\mu\alpha(\mathrm{Ra}\ \mathrm{Pr})^{1/2}} \tag{14}$$

These sets of equations in terms of the five unknowns, viz., u_x, u_r, u_θ, p, and T in the fluid and the porous region along with the appropriate boundary conditions, fully describe the buoyancy-driven flow in the annulus.

Boundary Conditions

Across the vertical symmetry plane there is no fluid flow and no heat transfer. The left and right end walls are assumed to be impermeable and insulated. The surface of the inner cylinder is maintained at a constant nondimensional temperature of unity, while that of the outer cylinder is held at a constant nondimensional temperature of zero. On all rigid and impermeable surfaces the three components of velocity are zero. The boundary conditions are summarized below.

For the left end wall

$$\text{at } x = 0 \text{ and } \frac{R_1}{R_2} \leqslant r \leqslant 1$$
$$u_x = u_r = u_\theta = 0 \qquad \frac{\partial T}{\partial x} = 0 \tag{15}$$

For the right end wall

$$\text{at } x = L \text{ and } \frac{R_1}{R_2} \leqslant r \leqslant 1$$
$$u_x = u_r = u_\theta = 0 \qquad \frac{\partial T}{\partial x} = 0 \tag{16}$$

For the vertical symmetry plane

$$\theta = 0^\circ \text{ and } \theta = 180^\circ$$
$$0 < x \leqslant \frac{L}{R_2} \text{ and } \frac{R_1}{R_2} \leqslant r \leqslant 1 \tag{17}$$
$$u_\theta = 0 \qquad \frac{\partial T}{\partial \theta} = 0$$

For the curved surface of the inner cylinder

$$\text{at } r = \frac{R_1}{R_2} \text{ and } 0 < x \leqslant \frac{L}{R_2}$$
$$u_x = u_r = u_\theta = 0 \qquad T = \frac{T_1 - T_\infty}{T_1 - T_\infty} = 1 \tag{18}$$

For the curved surface of the outer cylinder,

$$\text{at } r = \frac{R_2}{R_2} = 1 \text{ and } 0 < x < \frac{L}{R_2}$$
$$u_x = u_r = u_\theta = 0 \qquad T = \frac{T_2 - T_\infty}{T_1 - T_\infty} \tag{19}$$

FLUID FLOW

Background

The buoyancy-induced flow in the annulus between horizontal concentric cylinders of finite axial length has been previously studied [10]. It was found that a coaxial double-helical pattern was obtained. A given fluid particle introduced at one end of the annulus approached the central region of the annulus, drawing a small crescent-shaped vortex, and then turned around at the midaxial location and returned toward the end that it started from by drawing a larger crescent-shaped vortex outside the smaller one.

Iyer and Vafai [8] investigated the effects of the introduction of a geometric perturbation on the inner cylinder of the annulus and observed that there was a considerable change from the coaxial double-helical flow pattern. Iyer and Vafai [9] also studied the effect of multiple perturbations on the inner cylinder and observed that the introduction of each additional perturbation altered the flow field in a very regular manner. Considerable qualitative similarity was seen for the different cases involving different numbers of perturbations on the inner cylinder.

Flow Field Description

The main objective of this work is to investigate the validity of utilizing a porous perturbation for heat transfer augmentation within an annulus and also to study the effect of the introduction of a porous perturbation on the inner cylinder as opposed to a solid perturbation. Hence the description of the flow field will be made with respect to that for the annulus with a solid perturbation, which was presented in detail by Iyer and Vafai [8].

A comprehensive probe into the flow behavior was done, and a systematic approach was adopted to understand the nature of the flow field with the introduction of a porous perturbation. Velocity vectors at numerous axial positions along the annulus were carefully scrutinized with a view to physically visualize the nature of the flow field. Figure 2 shows the velocity vectors in the circumferential symmetry plane for the annulus with a porous perturbation. The velocity vectors are only discussed for the case in which $k_s/k_f = 500$, but similar trends were seen for the other cases considered. To better clarify the discussion, the annulus has been divided into three axial domains as follows: region A ($x = 0.0$–1.9), region B ($x = 1.9$–2.1), and region C ($x = 2.1$–4.0). A distinct feature of the flow field is the counterclockwise rotating cell formed near the top left end of the annulus. This feature is also observed for an annulus of finite axial length without a perturbation, and its formation can be attributed to the viscous effects at the left end wall.

For the case of an annulus with a solid perturbation, it was observed that the heated vertical portion of the perturbation caused the fluid in its vicinity to rise rapidly, thereby entraining fluid from the lower left and right ends of the annulus. Because of the impingement of the flow on the vertical walls of the perturbation, a portion of the flow is deflected back toward the axial ends of the annulus. A similar tendency was observed for the case of an annulus with a porous perturbation. The heated vertical portion of the perturbation entrained fluid into the upper circum-

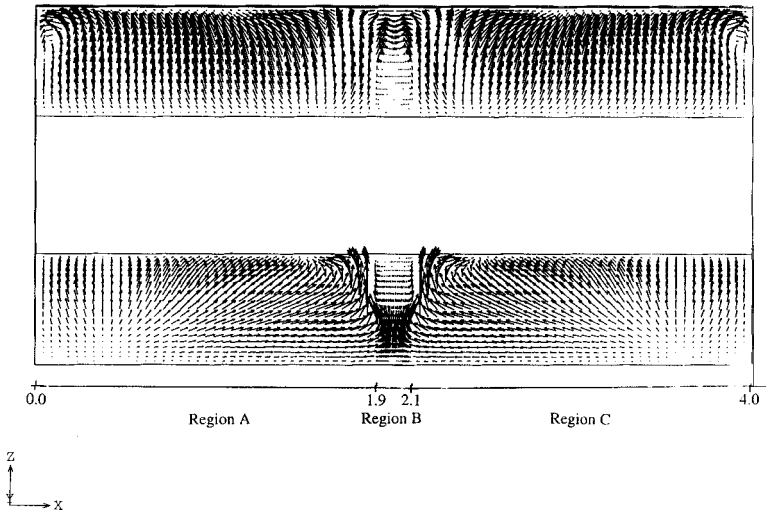

Figure 2. Velocity vectors in the circumferential symmetry plane for annulus with a porous perturbation.

ferential regime (Figure 2). However, because of the porous nature of the walls of the perturbation, the impingement of the flow did not cause a portion of the fluid entrained from region A and region C to move toward the left and right end walls, respectively. Another distinct departure from the previous case involved the circumferential regime over which the flow enters the narrow annular region formed between the perturbation and the surface of the outer cylinder. In the current case the flow was found to enter this narrow annular region predominantly through the upper circumferential region, unlike the previous case that involved flow entering the upper and lower extremes of the circumferential regime.

Within regions A and C, a stagnation zone in the upper circumferential regime is seen for a solid perturbation, but not so for a porous perturbation. This stagnant zone occurs due to the confluence of flow pockets [8]. One significant contributor to the formation of the stagnant zone is the flow that impinges on the vertical surface of the perturbation and gets deflected toward the left end wall. The absence of the stagnant zone can be attributed to the absence of this flow mode. However, similar stagnant zones were seen at lower ends of region A and region C for the porous and solid perturbations.

On the whole, a look at the magnitudes of the velocity vectors at different axial locations along the annulus reveals that for the same Ra, the presence of the porous perturbation alters the flow field considerably less than that corresponding to a solid perturbation. Also, for the case of an annulus with a porous perturbation, the buoyancy-induced flow field was seen to be less dominated by 3-D effects. For the porous perturbation cases, the flow pattern was 2-D over a large section of the annulus with the kidney-shaped flow circulation.

HEAT TRANSFER

To study the effect of inclusion of a porous perturbation on the temperature distribution, isotherms at numerous axial locations were looked at. At $\mathrm{Ra} = 10^3$ the heat transfer mechanism is dominated by conduction, and the temperature field is only slightly distorted by the convective field. Within the porous perturbation, the heat transfer is mainly by conduction. In the fluid region there are thermal boundary layers along the inner and outer cylinder surfaces, including a significant convective flow in this region.

Definitions

The local Nusselt numbers for the inner and outer cylinders are given by

$$\mathrm{Nu}_1 = \frac{h_1 D_1}{2k} \ln\left(\frac{D_2}{D_1}\right)$$
$$\mathrm{Nu}_2 = \frac{h_2 D_2}{2k} \ln\left(\frac{D_2}{D_1}\right) \tag{20}$$

where h_1 and h_2 are the local heat transfer coefficients on the inner and outer cylinders and are given by

$$h_1 = \frac{q_1}{(T_1 - T_2)} \quad \text{and} \quad h_2 = \frac{q_2}{(T_1 - T_2)} \tag{21}$$

respectively, where q_1 and q_2 are heat fluxes per unit area from the inner and outer cylinder surfaces, respectively. These nondimensional heat fluxes are given by

$$q = \frac{\partial T}{\partial n} \tag{22}$$

where n denotes the normal pointing outward from the surface over which the Nusselt number is to be calculated. The average Nusselt number over a surface area is given by

$$\overline{\mathrm{Nu}} = \frac{1}{A}\int \frac{\partial T}{\partial n}\, dA \tag{23}$$

Local Nusselt Number Distribution

Figure 3 shows the local Nu distributions on the inner and outer cylinder. The local Nu is plotted as a function of the circumferential and axial coordinates at $k_s/k_f = 500$ and $\mathrm{Ra} = 10^4$. With the introduction of a porous perturbation, the qualitative nature of the local Nu distribution was found to be very similar to that for an annulus with a solid perturbation, except in the region of the porous perturbation itself.

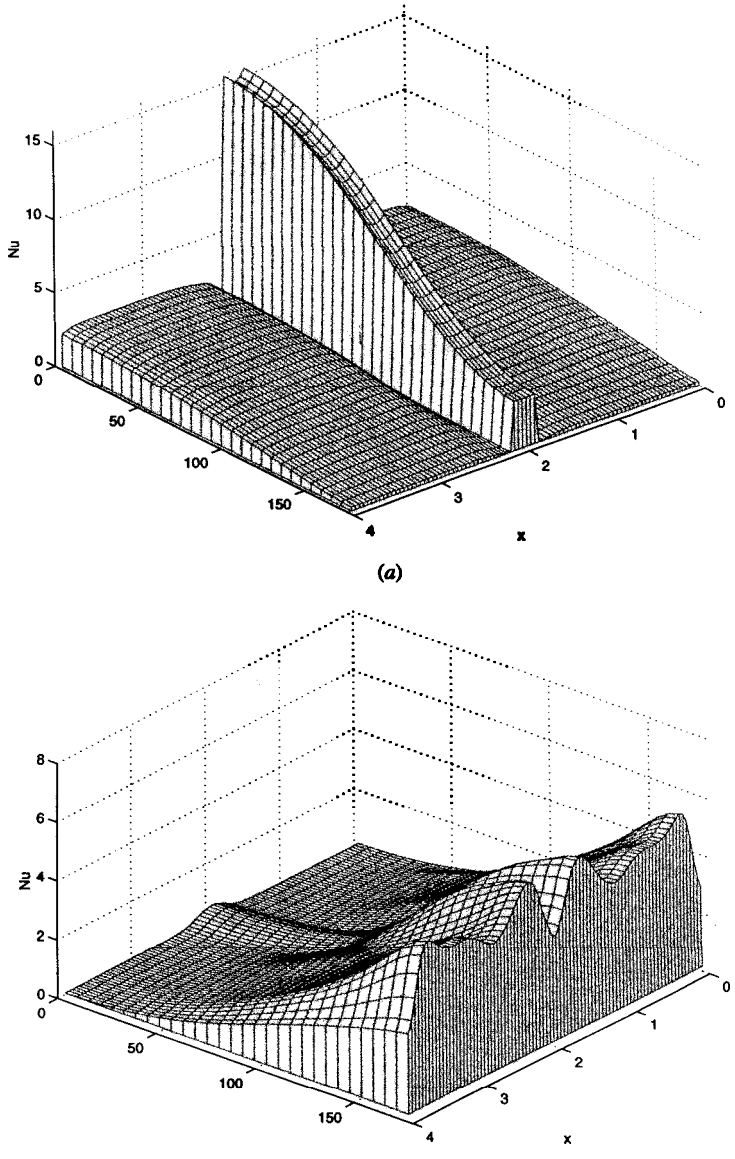

Figure 3. Local Nusselt number distribution at $\mathrm{Ra} = 10^4$ on (*a*) inner cylinder and (*b*) outer cylinder for annulus with a porous perturbation.

For the inner cylinder, Nu decreases steadily from the lower circumferential region to the upper circumferential region. In the vicinity of the porous perturbation, the local heat transfer rate, and hence Nu, on the inner cylinder are seen to increase sharply at the interface of the porous and the fluid region. This is due to the heat transfer enhancement by the porous substrate at this location. The

high-conductivity porous matrix offers a low-resistance path for the heat to dissipate from the surface of the inner cylinder.

For the outer cylinder the peaks at the axial extremities correspond to the circulatory cell generated by the viscous wall effects. In the vicinity of the porous perturbations the peaks in local Nu on the outer cylinder can be attributed to the flow entering the narrow annular region between the perturbation and the surface of the outer cylinder. The impingement of this buoyant jet causes the observed peaks.

Overall Heat Transfer Behavior

The effect of the thermal conductivity ratio is shown in Figure 4 for $\mathrm{Da} = 5 \times 10^{-5}$. The qualitative aspects of the results were found to be similar to those shown in Figure 4 for other Da. As expected, an increase in the conductivity ratio results in an increase in the average Nu. The heat transfer rate can be either greater than or less than the case where there is no perturbation on the inner cylinder, the determining factor being the conductivity ratio. For $k_s/k_f = 1.0$ the overall heat transfer rate was seen to be less than that for an annulus without a perturbation. With increasing conductivity ratio, the average Nu was found to

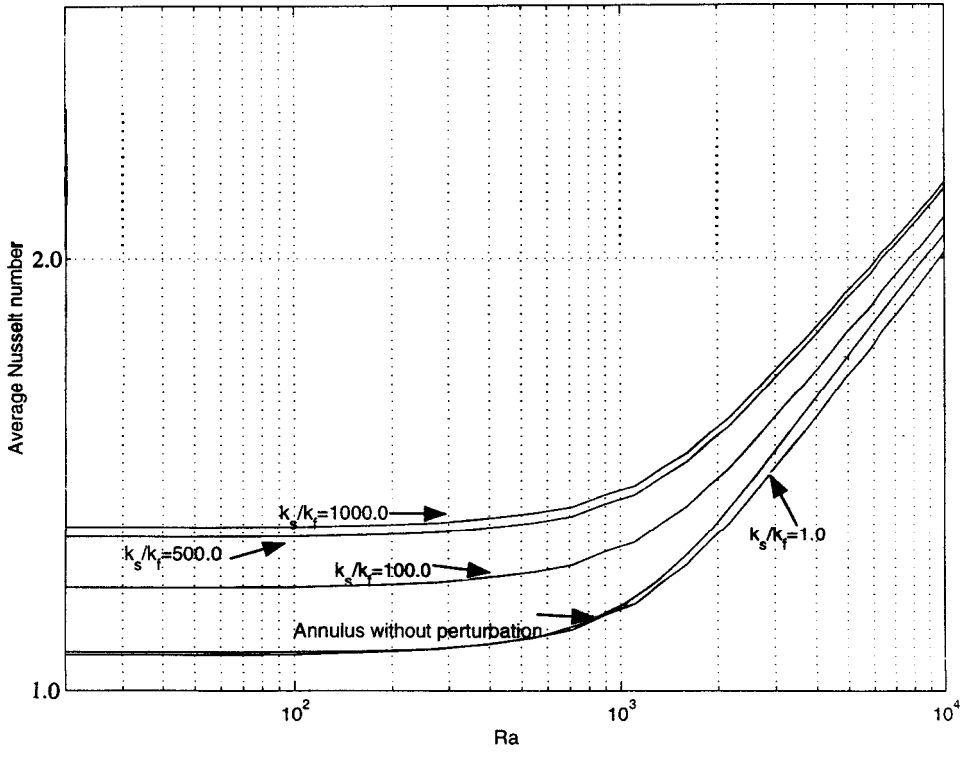

Figure 4. Effect of thermal conductivity on average Nusselt number.

increase at a progressively decreasing rate. Thus both heat transfer enhancement and retardation can be obtained through the addition of a porous perturbation on the inner cylinder. The average Nu at $\mathrm{Ra} = 10^4$ increased by 5.14% as k_s/k_f increased from 1 to 100, and by 4.67% as it increased from 100 to 500, while it increased by only 0.89% as k_s/k_f increased from 500 to 1000.

The study of the effect of permeability showed that with the presence of the porous matrix and/or the smaller value of permeability, smaller velocities resulted near the interface of the porous matrix and the surface of the inner cylinder. This, in turn, diminished the convective exchange of energy. For $\mathrm{Ra} = 10^4$ and $k_s/k_f = 100$ the average Nu decreased from 2.30 at $\mathrm{Da} = 5 \times 10^{-2}$ to 2.14 at $\mathrm{Da} = 5 \times 10^{-5}$.

The average Nu can be well correlated as a function of Ra, permeability, and conductivity ratio as follows:

$$\overline{\mathrm{Nu}} = 0.53\,\mathrm{Ra}^{0.14}\,\mathrm{Da}^{0.004}(k_s/k_f)^{0.02} \tag{24}$$

In order to study the effects of the inclusion of a porous as opposed to a solid perturbation, three conjugate cases involving solid perturbations were also analyzed. At any given value of k_s/k_f, the average Nu was found to be higher for the case involving a solid perturbation. At k_s/k_f values of 100, 500, and 1000 the average Nu at $\mathrm{Ra} = 10^4$ are found to be 2.14, 2.24, 2.26 and 2.25, 2.26, 2.27 for the porous and solid perturbations, respectively. At higher values of k_s/k_f the average Nu for the two cases are very close and at $\mathrm{Ra} = 10^4$, approach the value of 2.31, which was obtained for the case of the surface of the solid perturbation being maintained at the same temperature as that of the inner cylinder.

CONCLUSION

The effects of introducing a porous geometric perturbation on the buoyancy-driven flow and heat transfer in a cylindrical annulus and the possibility of heat transfer enhancement are investigated in this work. The geometry considered is a three-dimensional annulus whose inner and outer cylinders are isothermally heated and cooled, respectively, while the end walls are insulated. Detailed three-dimensional structure of the flow field and heat transfer characteristics have been analyzed and compared with those for a regular annulus without a perturbation as well as one with a solid perturbation. As compared to a regular annulus without a perturbation, the flow field was affected to a lesser degree with the introduction of a porous perturbation, as compared to the introduction of a solid perturbation. The qualitative effect of the introduction of either the solid or the porous perturbation was found to be very similar. Depending on the ratio of the conductivity of the porous material to that of the fluid, either heat transfer retardation or enhancement can be obtained. With decreasing permeability, the convective energy transfer was found to diminish. A correlation was presented accounting for the variation of the overall heat transfer as a function of the Rayleigh number, the Darcy number, and the solid to fluid conductivity ratio.

REFERENCES

1. Y. F. Rao, K. Fukuda, and S. Hasegawa, Steady and Transient Analyses of Natural Convection in a Horizontal Porous Annulus with the Galerkin Method, *J. Heat Transfer,* vol. 109, pp. 919–927, 1987.
2. I. Pop, D. B. Ingham, and P. Cheng, Transient Natural Convection in a Horizontal Concentric Annulus Filled with a Porous Medium, *J. Heat Transfer,* vol. 114, pp. 990–997, 1992.
3. M. C. Charrier-Mojtabi, A. Mojtabi, M. Azaiez, and G. Labrosse, Numerical and Experimental Study of Multicellular Free Convection Flows in an Annular Porous Layer, *Int. J. Heat Mass Transfer,* vol. 34, no. 12, pp. 3061–3074, 1991.
4. P. Vasseur, T. Hung Nguyen, L. Robillard, and V. K. Tong Thi, Natural Convection Between Horizontal Concentric Cylinders Filled with a Porous Layer with Internal Heat Generation, *Int. J. Heat Mass Transfer,* vol. 27, no. 3, pp. 337–349, 1984.
5. K. Muralidhar and F. A. Kulacki, Non-Darcy Natural Convection in a Saturated Horizontal Porous Annulus, *J. Heat Transfer*, vol. 110, pp. 113–139, 1988.
6. K. Vafai and S. J. Kim, Analysis of Surface Enhancement by a Porous Substrate, *J. Heat Transfer,* vol. 112, pp. 87–93, 1990.
7. J. Ettefagh, K. Vafai, and S. J. Kim, Non-Darcian Effects in Open Ended Cavities Filled with a Porous Medium, *J. Heat Transfer,* vol. 113, pp. 747–756, 1991.
8. S. V. Iyer and K. Vafai, Effects of a Geometric Perturbation on Buoyancy-Induced Flow and Heat Transfer in a Cylindrical Annulus, *Int. J. Heat Mass Transfer,* vol. 40, no. 12, pp. 2901–2911, 1997.
9. S. V. Iyer and K. Vafai, Buoyancy Induced Flow and Heat Transfer in a Cylindrical Annulus with Multiple Perturbations, *Int. J. Heat Mass Transfer,* vol. 41, pp. 3025–3035, 1998.
10. K. Vafai and J. Ettefagh, An Investigation of Transient Three-Dimensional Buoyancy-Driven Flow and Heat Transfer in a Closed Horizontal Annulus, *Int. J. Heat Mass Transfer,* vol. 34, pp. 2555–2570, 1991.